

# Design and Testing of an Experimental Magnetorheological Fluid Clutch

Zvonko HEROLD<sup>1)</sup>, Domagoj LIBL<sup>2)</sup> and Joško DEUR<sup>1)</sup>

1) Fakultet strojarstva i brodogradnje,  
Sveučilište u Zagrebu (Faculty of mechanical  
Engineering and Naval Architecture),  
Ivana Lučića 5, HR-10000 Zagreb  
**Republic of Croatia**

2) INETEC Institut za nuklearnu tehnologiju  
(Institute for Nuclear Technology),  
Dolenica 28, HR-10000 Zagreb,  
**Republic of Croatia**

zvonko.herold@fsb.hr

## Keywords

*Clutch  
Control  
Design  
Experimental analysis  
Magnetorheological fluid  
Testing*

## Ključne riječi

*Eksperimentalna analiza  
Ispitivanje  
Magnetoreološki fluid  
Projektiranje  
Regulacija  
Spojka*

**Received (primljeno):** 2010-04-28

**Accepted (prihvaćeno):** 2010-10-29

Original scientific paper

Owing to very good controllability, simple design, and durability, magnetorheological fluid (MRF) clutches become attractive solutions for various industrial and automotive applications. An experimental MRF clutch has been developed at the University of Zagreb, in order to support MRF clutch modeling, and control research. The clutch design facilitates MRF handling, change of fluid gap width, and testing various types of seals. The paper first presents calculation of the main clutch design parameters. Next, design of the overall clutch mechatronic system is described. Finally, the main results of testing the clutch static and transient behaviors are presented and compared with the design parameters.

## Projektiranje i ispitivanje eksperimentalne magnetoreološke spojke

Izvorno znanstveni članak

Zahvaljujući veoma dobrom svojstvu upravljanja, jednostavnoj konstrukciji i izdržljivosti, spojke temeljene na magnetoreološkim fluidima nalaze sve širu primjenu u industriji i tehnici motornih vozila. Eksperimentalna magnetoreološka spojka razvijena je na Sveučilištu u Zagrebu da bi se potakla istraživanja na području modeliranja i regulacije magnetoreoloških spojki. Spojka je konstruirana tako da olakša rukovanje fluidom, te omogući promjenu širine fluidnog raspora i primjenu raznih vrsta brtvi. Članak prvo izlaže proračun glavnih konstrukcijskih parametara spojke. Zatim se opisuje cjelokupni mehatronički sustav spojke. Konačno, prikazuju se glavni rezultati ispitivanja statičkog i dinamičkog ponašanja spojke, koji se uspoređuju s projektnim parametrima.

## 1. Introduction

The magnetorheological fluid (MRF) and related clutch devices were invented at the National Bureau of Standards by Jacob Rabinow in 1940s [1]. Rabinow proposed to use fine (micron-sized) iron particles suspended in fluid and exposed to the magnetic field. By changing the solenoid current, and thus the magnetic field, rheological properties of the MRF change, thereby resulting in the clutch torque change. The MRF clutches did not find their application until 1990s, because of practical difficulties related to particle settling, fluid thickening, and fluid sealing [2-3]. The R&D efforts in 1950s were, thus, turned to dry magnetic particle (MP) clutches, which were later used as standard industrial

clutches [4]. Once the MRF difficulties were resolved in the 1990s [3], the MRF clutches have again become an attractive solution because the fluid suspension prevents packing of magnetic particles and provides a smooth, silent, durable, and consistent behavior.

The main advantages of MRF clutches and brakes when compared with electrical motors include a superior torque/volume ratio (up to 10 times higher), high torque/inertia ratio, smooth torque response (no torque pulsations), and extremely small electrical power requirements (e.g. 10-20 W for torques of up to 100 Nm). Compared to frictional clutches, the MRF clutches are characterized by simpler design (due to purely electromagnetic actuation), better controllability (torque response is fast, repeatable, and proportional to current) and better durability (a

**Symbols/Oznake**

$A_{Fe1}$	- area of side part of yoke (column), m <sup>2</sup> - površina bočnog dijela jarma	$N$	- number of turns - broj zavoja
$A_{MRF}$	- active MR fluid area, m <sup>2</sup> - površina aktivnog dijela MR fluida	$N_{MRF}$	- number of MRF gaps - broj raspora s MR fluidom
$A_{Cu,sol}$	- active area of solenoid, m <sup>2</sup> - aktivna površina zavojnice	$NI$	- total magnetomotive force, A - ukupno magnetsko protjecanje
$A_{sol}$	- total area of solenoid, m <sup>2</sup> - ukupna površina zavojnice	$(NI)_{MRF}$	- magnetomotive force in MR fluid, A - magnetsko protjecanje u MR fluidu
$B_{Fe1}$	- magnetic flux density in steel, T - magnetska indukcija u željezu	$P$	- electric power, W - električna snaga
$B_{MRF}$	- magnetic flux density in MR fluid, T - magnetska indukcija u MR fluidu	$R$	- solenoid resistance, $\Omega$ - otpor zavojnice
$d_c$	- column width, m - širina bočnog dijela jarma	$R_o$	- outer radius of disk, m - vanjski polumjer diska
$d_{Fe}$	- slot width, m - širina magnetskog lima	$R_i$	- inner radius of disk, m - unutarnji polumjer diska
$d_y$	- yoke height, m - visina jarma	$\bar{R}_i$	- inner radius of MR fluid gap, m - unutarnji polumjer raspora s MR fluidom
$H_{MRF}$	- magnetic field in MR fluid, A/m - magnetsko polje u MR fluidu	$R_{iy}$	- outer radius of solenoid, m - vanjski polumjer zavojnice
$I$	- solenoid current, A - struja zavojnice	$r$	- radial coordinate, m - radijalna koordinata
$J$	- solenoid current density, A/m - gustoća struje zavojnice	$s$	- fluid gap width, m - širina raspora s MR fluidom
$K_{fring}$	- magnetic flux fringing factor - faktor rasipanja magnetskog toka	$T_{cc}$	- time constant due to the eddy current effect, s - vremenska konstanta vezana uz učinak vrtložnih struja
$K_{fil, sol}$	- solenoid filling factor - faktor popunjenosti zavojnice	$T_{el}$	- solenoid time constant, s - vremenska konstanta zavojnice
$L$	- solenoid inductance, H - induktivitet zavojnice	$W_{sol}$	- solenoid width, m - širina zavojnice
$l_{Fe1}$	- mean length of yoke, m - srednja duljina jarma	$\eta$	- fluid viscosity, Pa - viskozitet fluida
$l_{Fe2}$	- disk width, m - širina diska	$\rho_{Fe}$	- specific resistance of steel, $\Omega m^2/m$ - specifični otpor željeza
$l_{sol}$	- solenoid height, m - visina zavojnice	$\rho_{Cu}$	- specific resistance of copper, $\Omega m^2/m$ - specifični otpor bakra
$l_{sol, iso}$	- solenoid bed height, m - visina izolacijskog sloja zavojnice	$\tau_{yd}$	- yield stress, Pa - naprezanje tečenja
$M$	- clutch net torque, Nm - razvijeni moment spojke	$\Phi$	- polar angle, rad - polarni kut
$M_v$	- clutch viscous torque, Nm - viskozni moment spojke	$\omega$	- clutch slip speed, rad/s - brzina klizanja spojke

low level of wear). Typical industrial applications include devices comprising unwind/rewind, soft start, overload protection, and safe load holding operations [1, 4]. Characteristic automotive applications are active differentials [5–7], auxiliary engine devices such as fans [8], and steer-by-wire systems [9]. Besides the clutches/brakes, the MRF devices include active dampers that are used, for instance, in semi-active suspensions [9-10].

The MRF clutch design needs to satisfy quite opposite requirements on large torque/drag ratio, fast torque response, low power consumption, effective sealing, and stable operation without particle separation due to centrifuging [11]. Although a major part of clutch design can be conducted by using advanced, multi-physics, computer-aided design tools, the final design verification and possible modifications are based on extensive experimental tests.

This paper presents design of an experimental disk-type stationary MRF clutch (a brake) and related test rig, which have been primarily aimed at clutch modeling and control research [12-13]. The design provides ease of fluid manipulation, change of fluid thickness, and use of different fluid seals. The magnetic core is laminated to minimize the influence of eddy currents on the clutch torque response time [11,14]. The clutch is equipped with a tiny thermocouple and a magnetic flux sensor, which are placed near the fluid gap. The clutch rotor is driven by an electric servo-motor, while its stator is constrained by a precise force/torque sensor. By replacing the MRF medium by magnetic particles, the clutch may be used as an MP clutch.

The paper also presents the results of experimental characterization of the clutch static and dynamic behaviors. This includes the torque vs. current static curves, torque vs. speed curves, breakaway curves, current and torque transient responses, and thermal transient responses. The recorded curves are used to identify the main clutch static and dynamic parameters, which are then compared with the design parameters.

## 2. Clutch design

### 2.1. Calculation of clutch design parameters

The MRF clutch is to be tested by using resources of the existing experimental setup of internal combustion engine loaded by an electrical servo-motor [15]. The starting design parameters are, thus, determined by what follows:

- The rated clutch torque (for a linear torque vs. current static curve) should match the maximum torque  $M = 28$  Nm of the driving servo-motor,
- The inner radius  $R_i$  of active (magnetic) part of the clutch disk should not be smaller than 45 mm to provide adequate clutch connection to the servo-motor motor shaft (see Subsection 2.2).

The clutch design is based on the common equations for the clutch torque and electromagnetic quantities [11,16]. The clutch cross-sectional view is shown in Figure 1 (see Figure 5 for the clutch 3D drawing and photograph). The fluid MRF-132DG has been supplied by the Lord Corporation.

Choosing the inner and outer clutch disk radii  $R_i = 0,0465$  m and  $R_o = 0,0705$  m, respectively, gives the net torque

$$M = N_{\text{MRF}} \int_{R_i}^{R_o} \int_0^{2\pi} r \tau_{\text{yd}}(r, \Phi) r d\Phi dr = \frac{4\pi}{3} (R_o^3 - R_i^3) \tau_{\text{yd}} = 31,4 \text{ Nm}, \quad (1)$$

where  $N_{\text{MRF}} = 2$  is the number of MRF gaps and  $\tau_{\text{yd}} = 30000$  Pa is the Lord MRF-132DG fluid rated yield stress for the linear static curve (Figure 2a). Note that the realistic assumption of uniform yield stress distribution along the disk cross-sectional area is assumed ( $\tau_{\text{yd}} \neq f(r, \Phi)$ , non-uniformity of the magnetic field and the particle centrifuging effect are neglected [11]). The viscous torque (drag) is obtained as

$$M_v = N_{\text{MRF}} \int_{R_i}^{R_o} \int_0^{2\pi} r \eta \dot{\gamma} r d\Phi dr = \pi \frac{R_o^4 - R_i^4}{s} \eta \omega = 0,46 \text{ Nm}, \quad (2)$$

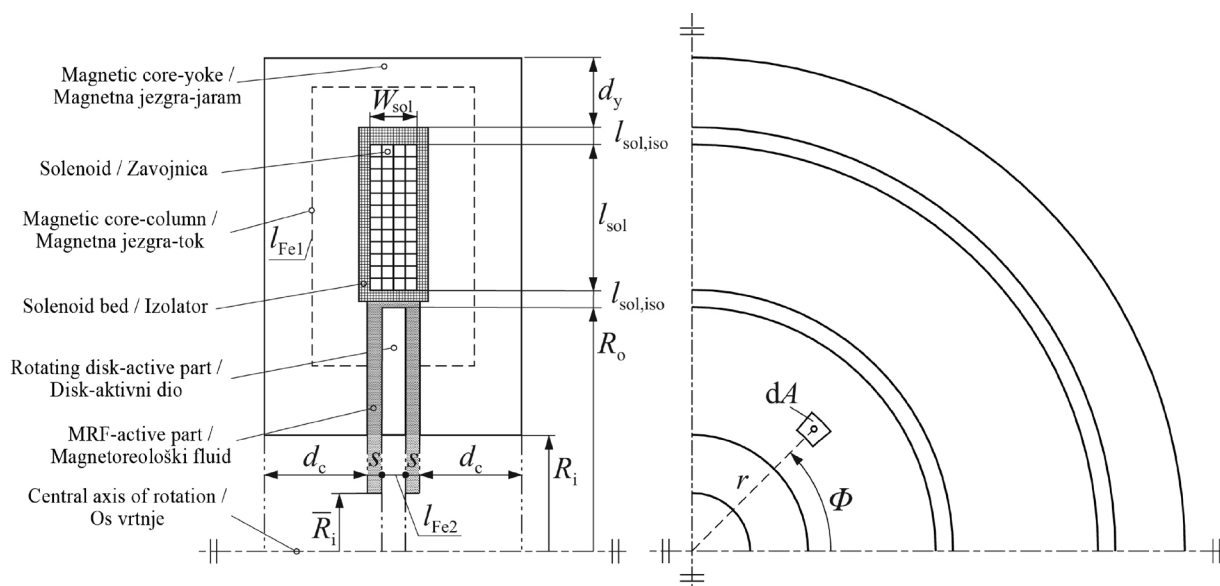
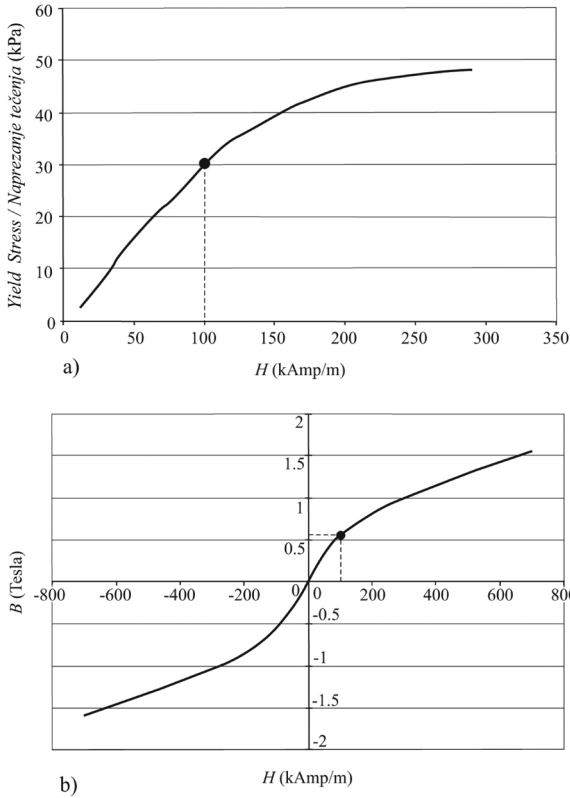


Figure 1. Cross-sectional views of MRF clutch active part  
Slika 1. Uzdužni presjek MRF spojke u radnom dijelu



**Slika 2.** MRF static curves [17] with operating point denoted  
**Slika 2.** Statičke karakteristike MRF [17] s prikazom statičke radne točke

where  $\dot{\gamma} = r\omega/s$  is the fluid shear rate,  $\eta = 0.12$  Pa is the fluid viscosity estimate [11],  $\omega = 100$  rad/s is the slip speed,  $s = 2$  mm is the fluid gap width, and  $\bar{R}_i = 0.025$  m is the true inner radius of the disk (active and inactive area, cf. Figures 1 and 5a). Note that the fluid gap width  $s$  is chosen to a minimum value of 2 mm that still prevents particle centrifuging [11].

The magnetomotive force (MMF) related to the rated magnetic field in the MRF gaps,  $H_{\text{MRF}} = 100 \cdot 10^3$  A/m (Figure 2a), is given by

$$(NI)_{\text{MRF}} = H_{\text{MRF}} N_{\text{MRF}} s = 400 \text{ A.} \quad (3)$$

In order to cover the MMF drops in magnetic core and slot lacquer, the total MMF is increased to  $NI = 568$  A

Based on a typical solenoid current density  $J = 4$  A/mm<sup>2</sup> and the solenoid filling factor  $K_{\text{fill,sol}} = 71$  %, the following net and total solenoid areas are obtained:

$$A_{\text{Cu,sol}} = NI / J = 142 \text{ mm}^2, \quad (4)$$

$$A_{\text{sol}} = A_{\text{Cu,sol}} / K_{\text{fill,sol}} = 200 \text{ mm}^2. \quad (5)$$

For the solenoid width  $W_{\text{sol}} = 8$  mm and the wire area  $A_{\text{Cu}} = 2.54$  mm<sup>2</sup>, this gives the solenoid length  $l_{\text{sol}}$  and the number of turns  $N$  (Figure 1):

$$l_{\text{sol}} = A_{\text{sol}} / W_{\text{sol}} = 25 \text{ mm}, \quad (6)$$

$$N = A_{\text{Cu,sol}} / A_{\text{Cu}} = 56. \quad (7)$$

The main solenoid electrical parameters are obtained as follows (note that  $l_{\text{iso,sol}} = 3.5$  mm, Figure 1; and  $\rho_{\text{Cu}} = 0.0175$   $\Omega$ mm<sup>2</sup>/m is the specific resistance of copper):

$$I = JA_{\text{Cu}} = 10 \text{ A}, \quad (8)$$

$$R = \rho_{\text{Cu}} \frac{2\pi(R_o + l_{\text{sol,iso}} + l_{\text{sol}}/2)}{A_{\text{Cu}}} N = 0,21 \Omega, \quad (9)$$

$$U = RI = 2,1 \text{ V}, \quad (10)$$

$$P = UI = 21 \text{ W}. \quad (11)$$

The solenoid inductance reads

$$L = \frac{NB_{\text{MRF}} A_{\text{MRF}}}{I} = 31 \text{ mH}, \quad (12)$$

where  $B_{\text{MRF}} = 0.6$  T is the rated magnetic flux density (Figure 2b) and  $A_{\text{MRF}} = K_{\text{fring}}(R_o^2 - R_i^2)\pi = 9,3 \cdot 10^{-3}$  m<sup>2</sup> is the active fluid area (Figure 1) with  $K_{\text{fring}} = 1,05$  denoting the magnetic flux fringing factor. The corresponding solenoid time constant  $T_{\text{el}}$  and the additional time constant due the eddy current effect [11],  $T_{\text{ec}}$ , are given by

$$T_{\text{el}} = L / R = 148 \text{ ms}, \quad (13)$$

$$T_{\text{ec}} \cong \frac{0,4 \cdot 10^{-3}}{\pi} \mu_{r0} \frac{d_{\text{Fe}}^2}{\rho_{\text{Fe}}} = 42 \text{ ms}, \quad (14)$$

where  $d_{\text{Fe}}$  [mm] is the thickness of laminated core slots,  $\mu_{r0} \cong 5000$  is the zero-field relative permeability of steel, and  $\rho_{\text{Fe}}$  [ $\Omega$ mm<sup>2</sup>/m] is the specific resistance of steel ( $\rho_{\text{Fe}} \cong 0.135$   $\Omega$ mm<sup>2</sup>/m). The slot width is chosen to  $d_{\text{Fe}} = 3$  mm to provide a reasonably small eddy-current time constant  $T_{\text{ec}} \ll T_{\text{el}}$ . Note that if the core were not laminated,  $T_{\text{ec}}$  would be very large (up to 1 s), which would substantially affect the clutch control performance (cf. [14]).

The column width  $d_c$  is obtained from the condition on equivalence of the magnetic flux in the MRF gap and the column (Figure 1):

$$A_{\text{MRF}} B_{\text{MRF}} = A_{\text{Fe1}} B_{\text{Fe1}} \cong 2\pi \frac{R_o + R_i}{2} d_c B_{\text{Fe1}},$$

which gives

$$d_c = \frac{A_{\text{MRF}} B_{\text{MRF}}}{(R_o + R_i)\pi B_{\text{Fe1}}} = 12,7 \text{ mm}, \quad (15)$$

for the the steel flux density chosen to  $B_{\text{Fe1}} = 1.2$  T.

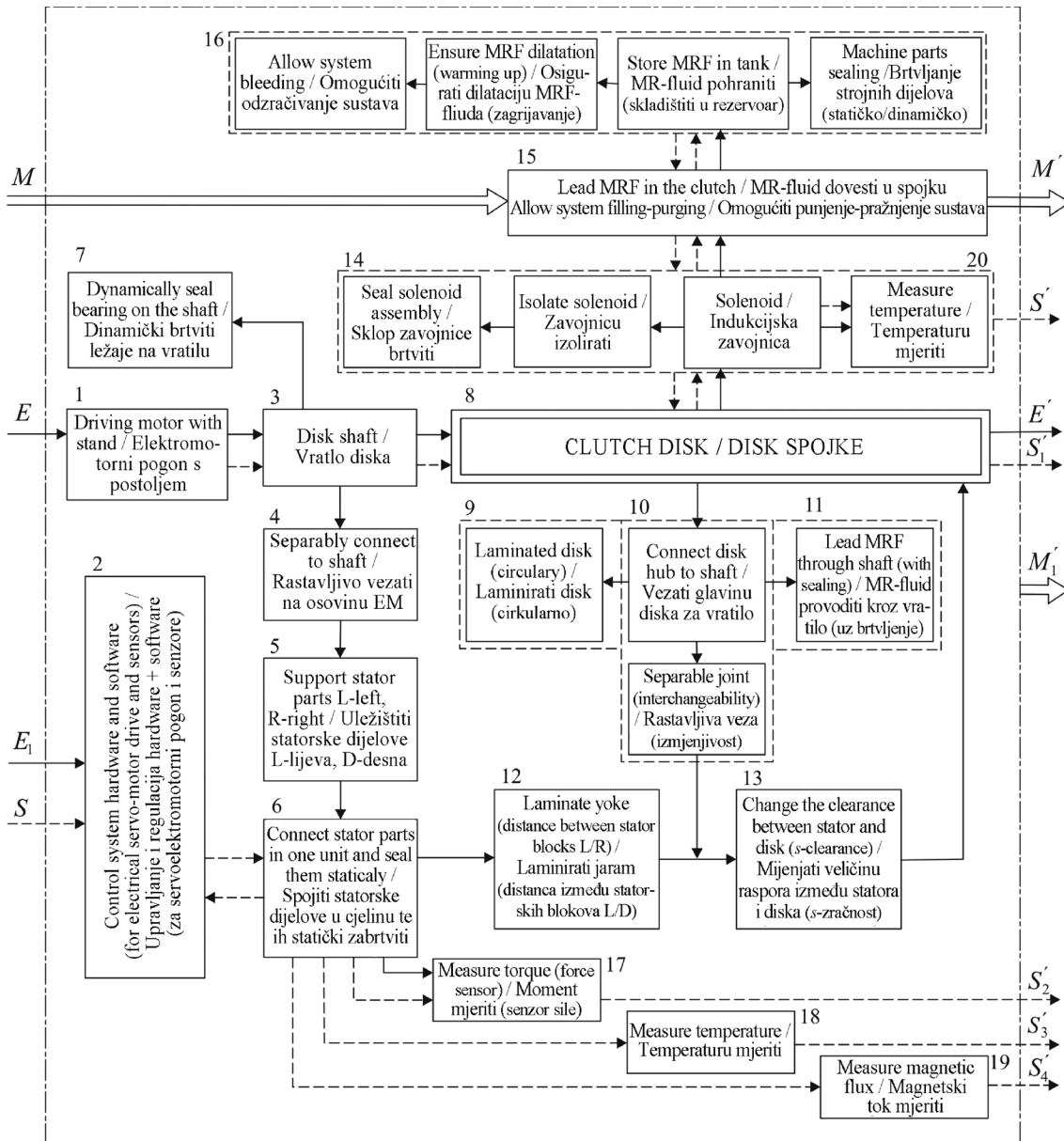


Figure 3. Overall functional structure of experimental system of MRF clutch (20 individual functions)

Slika 3. Ukupna funkcionalna struktura eksperimentalnog sustava MRF spojke ( 20 parcijalnih funkcija)

Similarly, the yoke height  $d_y$  is obtained from the condition (Figure 1):  $A_{Fe1} B_{Fe1} = ((R_{iy} + d_y)^2 - R_{iy}^2) \pi B_{Fe1}$  with  $R_{iy} = R_o + l_{sol} + 2l_{sol,iso} = 102,5$  mm.

This leads to the square equation

$$d_y^2 + 2R_{iy}d_y - (R_o + R_i)d_c = 0, \tag{16}$$

with the solution

$$d_y = 7 \text{ mm.}$$

Thus, each column is composed of four slot pairs each with the width of 3 mm, and the yoke includes two slots (rings) with the height of 3.5 mm (see Figure 5a). The disk is also slotted by using six rings with the height

of 4 mm (Figure 5a). The slots are isolated by a lacquer. The ring slots are cut in the radial direction to suppress the eddy currents.

### 2.2. Mechanical subsystem

The MRF clutch was designed by using a methodical approach of design in order to achieve a best possible solution. For that purpose the design process is defined by an overall function/structure, as well as the environment which defines input and output connections. In the initial design stage, the overall clutch function is divided into partial functions of lower complexity, which, when joined

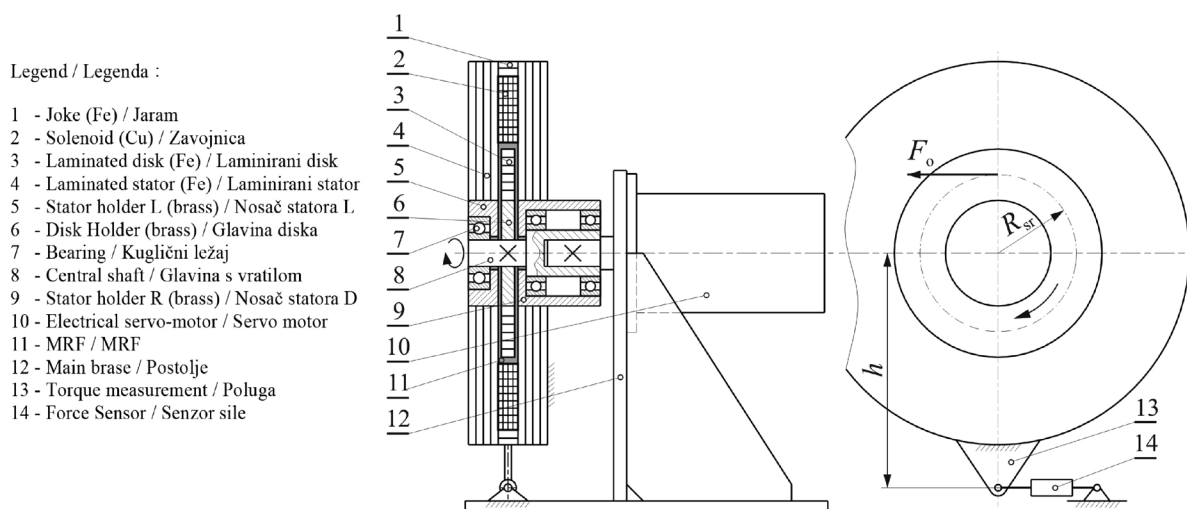


**Figure 4.** Conceptual solution of experimental MRF clutch

**Slika 4.** Konceptijsko rješenje eksperimentalnog postava MRF spojke

together through relations, give the overall clutch system functional structure (Figure 3). This functional structure enables more alternatives of the conceptual solution to be found and created. However, only the implemented solution is presented here, which is based on the use of an existing servo-motor to drive the experimental clutch.

The final conceptual solution is shown in Figure 4. The sequence of design process elaboration and form solutions of all partial functions (functions 1 to 20 in Figure 3) is shown by the 3D model cross-section in Figure 5. In the final conceptual solution, the clutch hub is mounted directly on the driving motor shaft (13). The connection is realized by a radial pin. The clutch hub carries the laminated rotor disk (10) and the clutch stator assembly bearing (14). The clutch stator assembly consists of the laminated armature (made from transformer sheets) (7) and the isolated induction coil (16) connected by bolts passing through the stator flange (1). The stator is fixed to the overall setup base through the lever (9) and the force sensor (8). In this way, the MRF clutch is turned into a brake, where the transferred torque is measured as the reactive braking torque. Such clutch design is somewhat complex and more demanding, but on the other hand, the overall experimental system design is rather cost-effective, because of using the existing driving motor with related control hardware and software. Furthermore, the primary objective of the considered MRF clutch is to present an experimental clutch setup, which assumes providing variability of the main operating parameters. In order to meet these requirements, the design allows for replacement of the laminated disk in order to provide variation of the MRF gap width and manipulation with the MRF by sucking it into an external tank by using a manual pump mechanism.

### 2.3. Fluid handling subsystem

The MRF should be easily delivered into the space between the laminated stator core and the disk without presence of air bubbles. On the other hand, the MRF should be simply sucked out from the clutch prior to disassembling the left side of the stator assembly and replacing the disk to change the MRF gap width parameter  $s$ . The internal flow of the MRF is illustrated in Figure 6. When the system is filled, the fluid is seen on the upper bleeding vent, and the external tank is then disconnected and both vents are closed. The possibility of MRF thermal dilatation is ensured by means of a central cylinder with a piston and a spring. Some of the stator parts and also the disc hub with central shaft are connected with bolted connections through flanges, in order to allow fast and effective parts replacement. During every disassembly, disc replacement, and reassembly, specific care must be dedicated to correct gasket positioning. There are two basic sealing methods used in the system (Figure 7): static sealing with O-rings made from PTFE and dynamic sealing based on simmering type seals made of Simrit PTFE.

### 2.4. Electrical and control subsystem

The MRF clutch is driven by an electrical servo-motor of permanent-magnet synchronous type (Figure 5b). The maximum speed and torque are 4000 rpm and 28 Nm, respectively. The clutch motor is normally used in the closed-loop speed control mode (10 Hz bandwidth), but open-loop torque/current control (80 Hz bandwidth) can also be used in some experiments (e.g. the breakaway experiment, Section 3). The motor/clutch position measurement resolution is 0.09 deg. The speed signal is obtained by time differentiation of the position signal. The speed measurement resolution is 1.5 rad/s.

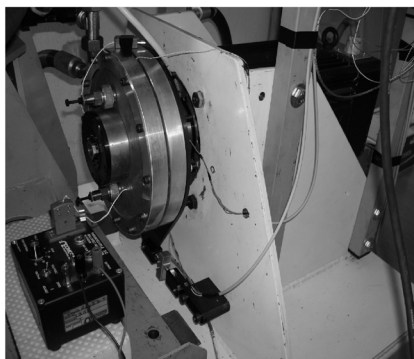
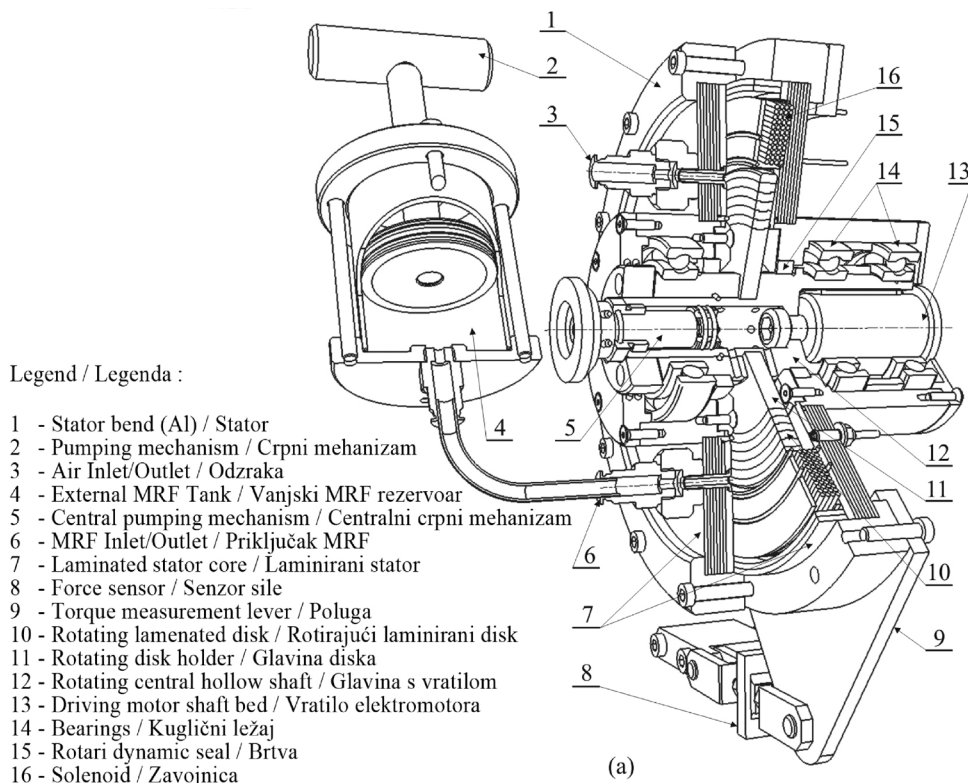


Figure 5. 3D drawing (a) and photograph (b) of experimental MRF clutch

Slika 5. 3D crtež (a) i fotografija (b) eksperimentalnog postava MRF spojke

The clutch torque is measured by a lever system that connects the clutch case to a strain-gauge force sensor. The clutch itself is equipped by tiny thermocouple and magnetic flux sensors by OMEGA and F.W. BELL, respectively, which are mounted in the side slot nearby the MRF gap (Figure 5a). A PTC temperature sensor is inserted into the solenoid bed.

The clutch solenoid is supplied from a four-quadrant 24V/50A MOSFET chopper. The chopper is connected to two standard 12 V automotive batteries connected in series (24 V power supply), and it comprises a fast Hall-effect current sensor by LEM. The measured current signal is fed back to a Pentium III industrial computer

that controls the chopper. The same computer controls the frequency converter that supplies the driving servomotor. The control computer is equipped with analog input/output and encoder data acquisition cards. The control code is written in C under the DOS operating system. The sampling time is 1 ms.

Figure 8 shows the block diagram of the clutch current control system. The difference of reference current  $i_R$  and the measured current  $i$  is fed to a proportional-integral (PI) controller. The controller commands the clutch voltage reference signal  $u_R$ , which is realized through the chopper ( $u = K_{ch} u_R$ ,  $K_{ch} = 24/5 = 4,8$  V). The pure delay  $T_\Sigma = 1,4$  ms includes the delays due to time-

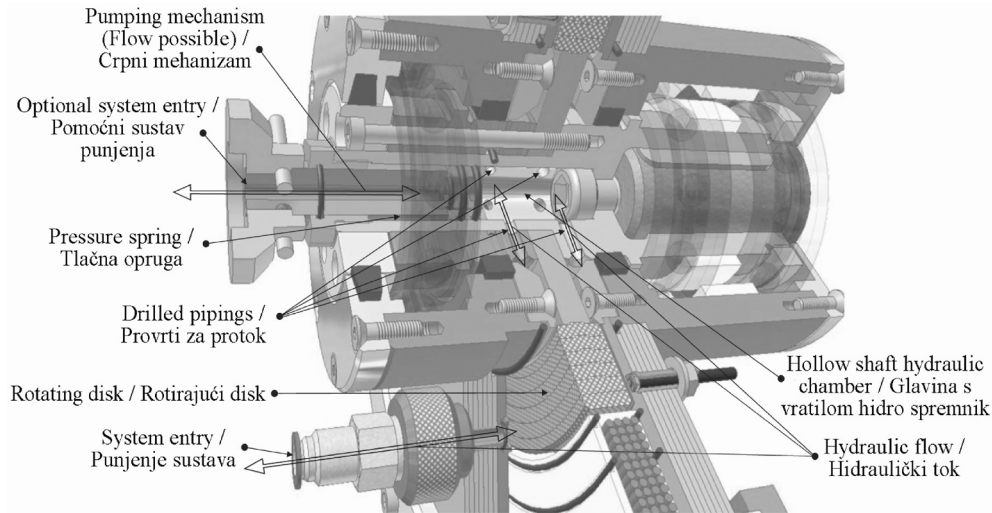


**Figure 6.** MRF Circuit – internal MRF flow  
**Slika 6.** Kruženje MRF – unutrašnji tok fluida

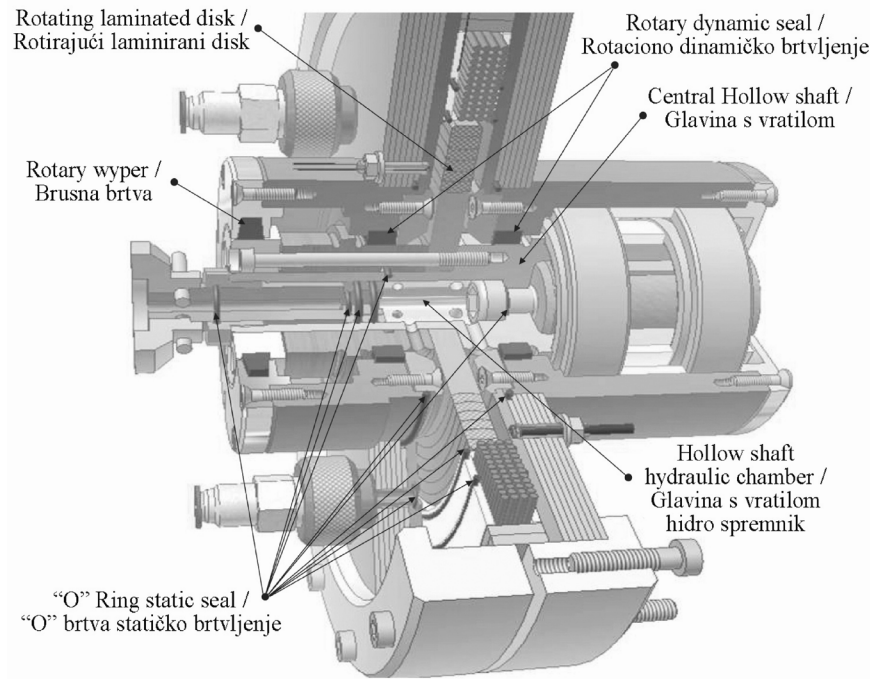


**Figure 7.** MRF Circuit – static and dynamic seals  
**Slika 7.** Kruženje MRF – statičko i dinamičko brtvljenje

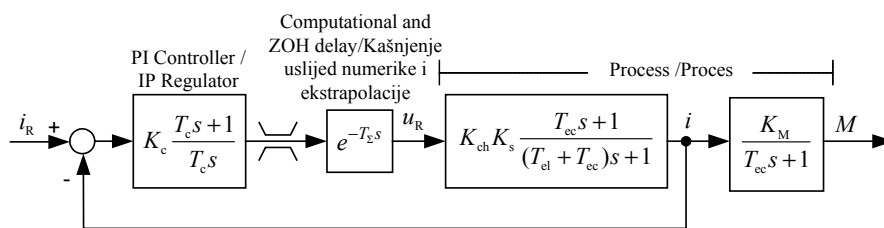


**Figure 8.** Block diagram of clutch current control system  
**Slika 8.** Blokovski dijagram regulacijskog kruga

discretization, speed measurement, and control algorithm computation. The process model transfer functions  $i(s)/u_R(s)$  and  $M(s)/i(s)$  are obtained from a transformer-like clutch model including the eddy current effect [12-13]. The current response  $i(t)$  is faster than the torque response  $M(t)$ , because of the presence of lead time constant  $T_{cc}$  in

the transfer function  $i(s)/u_R(s)$ . The PI controller is tuned according to the technical optimum criterion [18], where  $T_c = T_{el}$  is chosen to speed up the current response and the gain  $K_c$  is set to provide the fastest aperiodic current response (see [12] for more detail on control system design).



### 3. Clutch testing

Results of testing the clutch static and transient behaviors are presented in this section. The test results have been used in [12] for parameterizing and validating the clutch dynamics model.

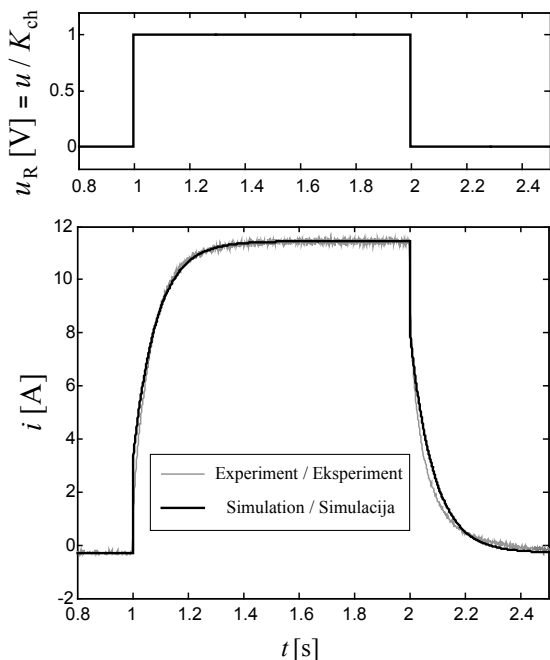


Figure 9. Clutch current response with respect to stepwise voltage change

Slika 9. Vremenski odziv struje na skokovitu promjenu napona

#### 3.1. Current and torque transient responses

The clutch current response  $i(t)$  with respect to stepwise change of the commanded voltage  $u_R$  is shown

in Figure 9. A good agreement between the experimental and computer-simulation responses indicates that the lead-lag transfer function model  $i(s)/u_R(s)$  in Figure 8 can accurately describe the clutch current response. The identified model parameters are:  $K_s = 1/R = 2,4 \Omega^{-1}$ ,  $T_{el} = 60 \text{ ms}$ ,  $T_{ec} = 25 \text{ ms}$ . The identified resistance  $R = 1/K_s = 0,42 \Omega$  is larger than the theoretical solenoid resistance value  $R^* = 0,21 \Omega$  (Subsection 2.1), because of the influence of battery, wire, and MOSFET resistances. Also, the flux density is reduced from its theoretical value ( $B = s^*/s \cdot B^*$ ; see Eq. (3) and Figure 2b) due to the increase of MRF gap from  $s^* = 2 \text{ mm}$  to  $s = 3 \text{ mm}$ . Accordingly, the electrical time constant given by Eq. (13) should be corrected as  $T_{el} = (s^*R) / (sR) \cdot T_{el}^* = 49 \text{ ms}$ , which is in a good agreement with the identified value of 60 ms. The identified eddy-current time constant  $T_{ec} = 25 \text{ ms}$  is in a reasonable agreement with the roughly predicted value of 42 ms based on Eq. (14).

Figure 10 shows the closed-loop current responses and the corresponding normalized clutch torque responses with respect to different magnitudes of current reference ( $i_R$ ) step change. The current response is very fast in accordance with the small closed-loop time constant achieved ( $T_{eq} = 6 \text{ ms}$ ). On the other hand, the clutch torque response is slower due to the effect of eddy current lag term  $1 / (T_{ec}s + 1)$  that remains outside the current control loop (Figure 8). The torque response settling time is around 50 ms. Comparison of the simulation and experimental responses in Figure 10 further confirms the accuracy of linear current model in Figure 8. However, the torque model is rather inaccurate for the torque off phase. Namely, the experimental response is initially steep, which is also seen in the magnetic flux sensor response (Figure 11). In addition, the torque model exhibits a steady-state inaccuracy in the case of non-zero initial current (see the lowest subplot in Figure 10). Both

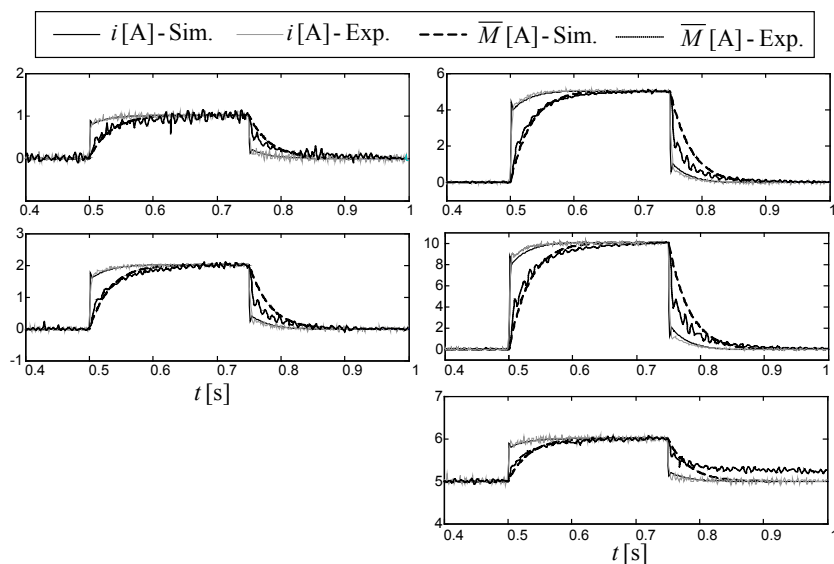


Figure 10. Step responses of current control closed-loop system, including normalized torque responses

Slika 10. Vremenski odziv regulacijskog kruga struje na skokovitu promjenu referencu uključujući normirani odziv momenta

inaccuracies are predominantly caused by the nonlinear effect of magnetic hysteresis (see next subsection), and they can be largely reduced by using a nonlinear model of the clutch electromagnetic circuit, as proposed in [13].

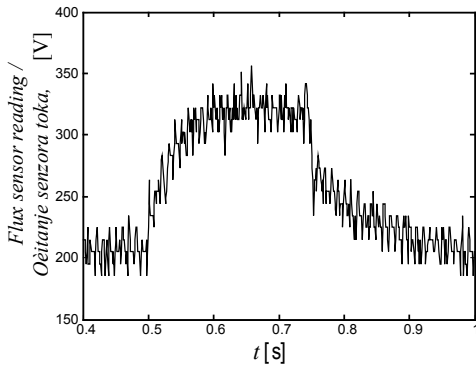


Figure 11. Magnetic flux sensor reading during the current control system step response ( $i: 0 \rightarrow 5\text{A}$ ) from Figure 10

Slika 11. Vremenski odziv senzora magnetskog toka na skokovitu promjenu reference struje ( $i: 0 \rightarrow 5\text{A}$ ) prikazanog na slici 10

### 3.2. Static curves

#### 3.2.1. Torque vs. current curves

Executing the quasi-steady-state closed-loop experiment with zero initial current (see the very top subplot of Figure 12) has given the net-torque vs. current static curves shown in Figure 12a. The static curves for non-zero initial current are shown in Figure 12b. As projected by the design (Subsection 2.1, Figure 2a), the static curves in Figure 12a have a linear shape. The rated net torque of 20,5 Nm agrees very well with the scaled theoretical value  $M' = s/s^2 \cdot M = 20.9\text{ Nm}$  obtained from Eq. (1). The static curves in Figure 12 include hysteric loops caused by the magnetic hysteresis. The higher the current amplitude, the narrower the hysteresis. For the non-zero initial current, the torque is somewhat different for the same current depending on whether the current is growing or falling (see Figure 12b and the related discussion on steady-state inaccuracy of torque control from Subsection 3.1).

Static curve points above the rated current of 10 A can be recorded by using a clutch stopping experiment illustrated in the top subplot of Figure 13 (note that the motor torque was not large enough for the static experiment). The results in Figure 13 show that the clutch torque can be significantly increased over the rated one, which is partly due to the increased MRF gap  $s^2/s = 1,5$  and partly due to the torque reserve in the MRF static curve in Figure 2a.

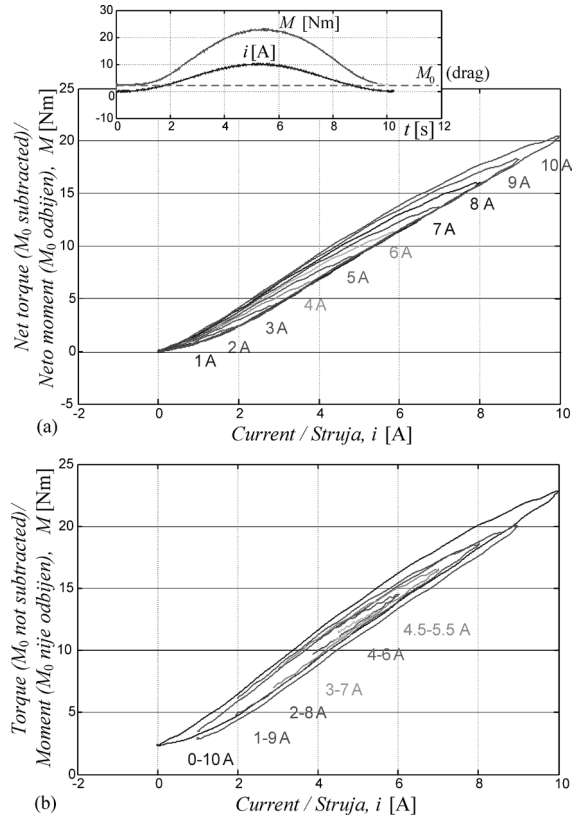


Figure 12. Torque vs. current static curves ( $\omega = 100\text{ rpm}$ )

Slika 12. Statička karakteristika momenta u ovisnosti o struji ( $\omega = 100\text{ min}^{-1}$ )

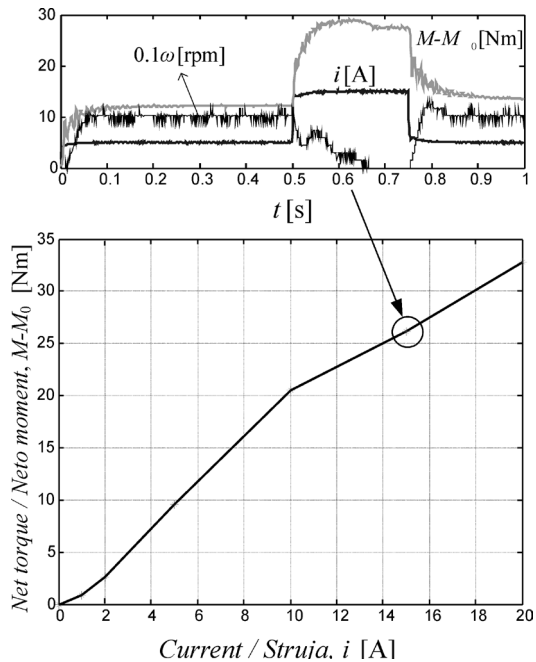


Figure 13. Extended torque vs. current static curve

Slika 13. Proširena statička karakteristika momenta u ovisnosti o struji

3.2.2. Torque vs. speed curves

Figure 14 illustrates the quasi-static experiment used to record the clutch torque vs. speed curves. The current is constant ( $i = 10 \text{ A}$ ) and the clutch speed is controlled by the driving servo-motor to have an inverted cosine profile. The recorded torque curve exhibits a narrow hysteresis, which is predominantly caused by the fluid viscosity variations due to temperature change. The torque curve part corresponding to the negative sign of speed derivative ( $\text{sgn } d\omega/dt < 0$ ) is taken as a more representative one, because the related temperature curve is more flatter then. The final torque vs. speed curves recorded for different currents are shown in Figure 15. These curves are in a good agreement with the data obtained from the static curve in Figure 12a for the speed of 100 rpm (see the points marked with symbol \* in Figure 15).

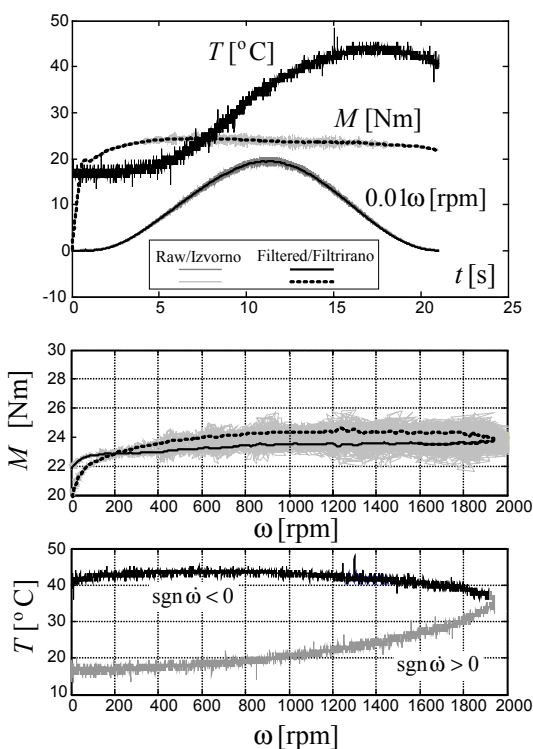


Figure 14. Quasi-static experiment used to record torque vs. speed static curve ( $i = 10 \text{ A}$ )

Slika 14. Dijagrami kvazi-statičkog eksperimenta korištenog za snimanje statičke karakteristike momenta spojke ( $i=10 \text{ A}$ )

The static curves in Figure 15 have the well-known form of Coulomb+viscous friction [19]. The main difference when compared to the traditional friction clutches is that the torque can be precisely controlled electrically (by changing the current instead of the normal force). After subtracting the current-dependent net torque and the zero-speed torque (clutch bearing dry friction) from the static curves in Figure 15, the viscous friction curves shown in Figure 16 are obtained. These curves are

linear in  $\log\omega$  scale for  $\omega < 100 \text{ rpm}$ , and approximately linear in  $\omega$  scale for  $\omega > 100 \text{ rpm}$ . Although a relatively modest viscous-torque data scattering can partly be contributed to the temperature effect, the curves in Figures 15 and 16 show the following general trends which are in agreement with the results from [11]: (i) the zero-current viscous torque rises more than linearly for  $\omega > 1000 \text{ rpm}$ , and (ii) the fluid magnetization results in flattening the viscous torque curve. The viscous torque at the speed of  $1000 \text{ rpm} \cong 100 \text{ rad/s}$  is approximately equal to  $0,9 \text{ Nm}$ . This exceeds the theoretical value  $M^* = s/s^* \cdot M_v = 0,31 \text{ Nm}$  based on Eq. (2), which is explained by the bearing viscous friction influence (not compensated in Figure 16), and an inaccurate value of the fluid viscosity  $\eta$ .

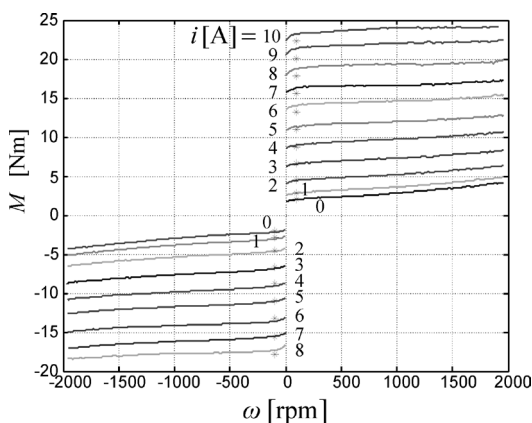


Figure 15. Torque vs. speed static curves

Slika 15. Statičke karakteristike moment spojke

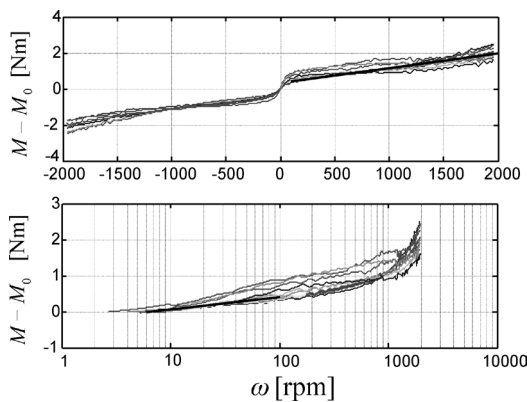


Figure 16. Viscous torque static curves in linear and logarithmic speed scale

Slika 16. Statičke karakteristike viskoznog trenja u linearnom i logaritamskom mjerilu

3.3. Micro-slip behavior

The quasi-static experiment for a lower speed range (from 0,2 to 10 rpm) are shown in Figure 17. According to the trends observed in Figures 15 and 16, the torque tends to slightly decrease with speed decrease. The torque

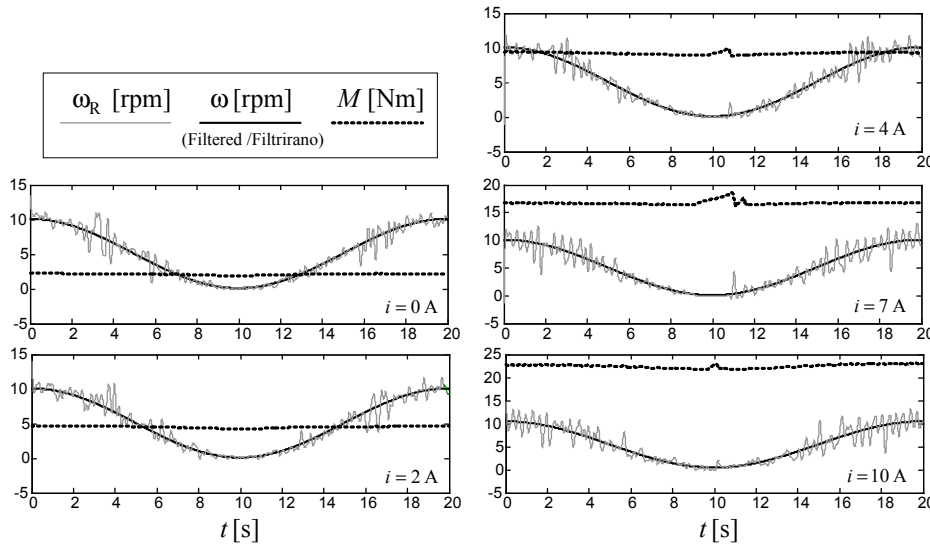


Figure 17. Quasi-static experiment results in low-speed (Stribeck) region

Slika 17. Vremenski dijagrami kvazi-statičkih eksperimenata u području malih brzina klizanja (Stribekovo područje)

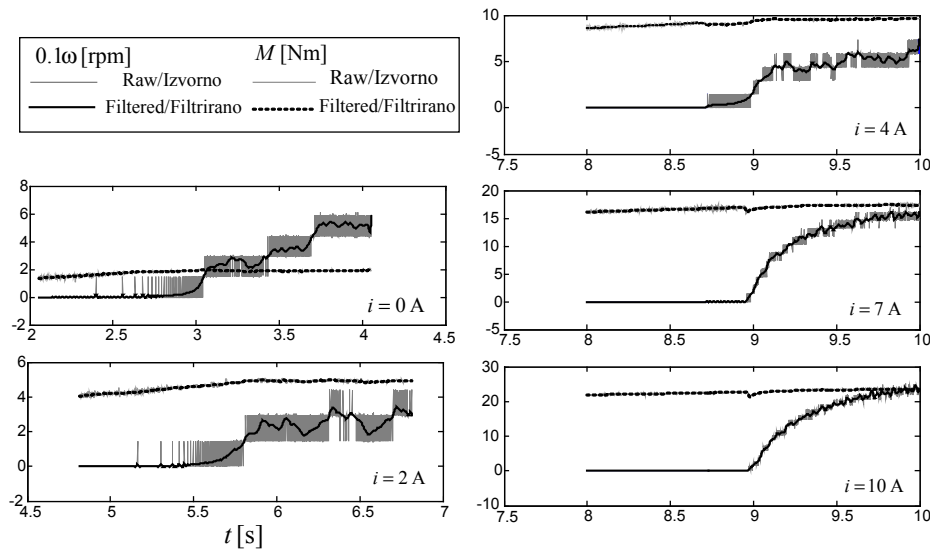


Figure 18. Breakaway test results

Slika 18. Vremenski dijagrami eksperimenata odvajanja

is smooth and the speed is precisely controlled for small clutch currents ( $i \leq 2$  A). However, at larger currents the torque can abruptly increase towards stiction value, the clutch temporarily locks, and a stick-slip behavior can occur. This effect corresponds to the falling Stribeck friction curve [19]. The zero-speed torque decay is steep, i.e. the stiction torque excess vanishes at very small speeds.

Figure 18 shows the results of a clutch breakaway experiment for different clutch currents. In this experiment, the locked clutch with a constant current is exposed to a slow linear rise of the driving motor torque until the clutch breakaways and exceeds a predetermined small speed threshold. Again, the clutch torque breakaway transition is smooth for the small currents ( $i \leq 2$  A), while an abrupt, though small-magnitude stick-slip torque drop occurs at larger currents.

Figure 19 indicates that the clutch used in this paper does not exhibit a presliding motion when exposed to

the driving motor torque rise under the locked clutch conditions. More precisely, the presliding displacement (as observed in [11]) is here less than the position measurement resolution of  $0,09^\circ$ , i.e. the locked clutch torsional stiffness is larger than  $12700$  Nm/rad.

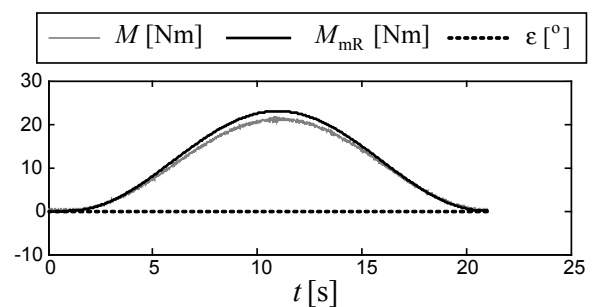
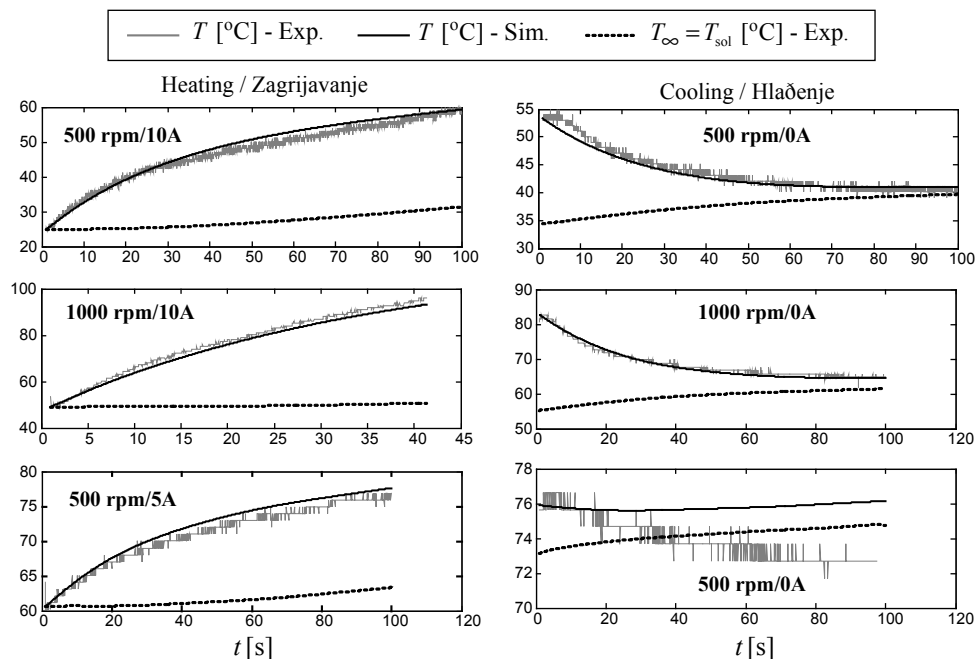


Figure 19. Presliding displacement experiment response  
Slika 19. Vremenski dijagram relativnog pomaka u fazi držanja



**Figure 20.** Thermal transient responses  
**Slika 20.** Vremenski odzivi temperature spojke

### 3.4. Thermal transients

Figure 20 shows the clutch thermal transients for various engaged-clutch (heating) and open-clutch (cooling) conditions. The measured fluid temperature during the cooling condition points out that the fluid thermal time constant is around 30 s. Simulation results indicate that the MRF temperature transients can accurately be predicted by a simple first-order thermal model [12], which is based on the heat balance equation with a constant heat transfer factor and the solenoid temperature used as the environment temperature. Note that the (relatively slow) clutch case/solenoid temperature rise, observed in Figure 20, limits the clutch thermal capacity or the duty cycle. For the heavy-duty operating conditions, it can, thus, be important to implement a clutch cooling system (see e.g. [7]).

## 4. Conclusion

An experimental MRF clutch has been designed for the purpose of clutch dynamics modeling and control research, as well as for gaining experience in designing the MRF devices. For the purpose of a detailed experimental characterization and model validation, the clutch is equipped with various sensors and driven by an electric servo-motor. In order to reach a high level of clutch testing flexibility, the clutch design facilitates MRF handling/replacement, change of fluid gap width, and testing various types of seals.

The clutch static and dynamic behaviors have been experimentally characterized, in order to validate the clutch design and provide a basis for the clutch

model development. Owing to a slotted design of the magnetic core, a fast clutch torque response has been achieved (the torque response settling time is around 50 ms). The torque vs. current static curve is linear, when neglecting a modest magnetic hysteresis effect. The hysteresis becomes narrower for the lower current/torque amplitudes. The experimentally identified rated torque and the main time constants agree well with the corresponding design values. The clutch viscous torque exhibits an approximately linear rising dependence on the clutch slip speed for speeds larger than 100 rpm, while the dependence is logarithmic for lower speeds. A falling Stribeck curve (stick-slip curve) has been identified for medium-large currents/torques, where the Stribeck torque excess is up to 10%. The traditional first-order thermal transient model, with a constant heat transfer coefficient and the ambient temperature equal to the solenoid temperature, can predict accurate MRF temperature responses for the monitoring purposes.

## Acknowledgment

It is gratefully acknowledged that this work has been supported by Jaguar Cars Ltd., and partly by the Ministry of Science, Education, and Sports of the Republic of Croatia. The authors' appreciation also goes to Dipl. Ing. Anton Lisac, NEV-EL, Zagreb, Prof. Zlatko Maljković and Dr. Milan Kostelac, University of Zagreb, and Zoran Milojković, M.Sc., Končar, Zagreb, who provided technical support and helpful suggestions related to clutch design, as well as to Dr. Danijel Pavković and Dipl. Ing. Mario Hrgetić for their help in electrical hardware and software implementation.

## REFERENCES

- [1] RABINOW, J.: *The Magnetic Fluid Clutch*, AIEE Transactions, Vol. 67, pp. 1308-1315, 1948.
- [2] JOLLY, M. R.; BENDER, J.W.; CARLSON, J.D.: *Properties and Applications of Commercial Magnetorheological Fluids*, SPIE 5th Annual Int. Symposium on Smart Structures and Materials, San Diego, CA, 1998.
- [3] CARLSON, J. D.: *What Makes a Good MR Fluid?*, 8th Int. Conf. on Electrorheological (ER) Fluids and Magneto-rheological (MR) Suspensions, Nice, France, 2001.
- [4] EDDENS, G. R.: *Magnetic Particle Clutches and Brakes: A primer*, Power Transmission Design, Vol. 20, No. 3, pp. 59-61, 1978.
- [5] WHEALS, J. C.; Baker, H.; Ramsey, K.; Turner, W.: *Torque Vectoring AWD Driveline: Design, Simulation, Capabilities and Control*, SAE paper No. 2004-01-0863, 2004.
- [6] GRATZER, F.; STEINWENDER, H.; KUŠEJ, A.: *Magnetorheological AWD Clutches*, ATZ, Vol. 110, No. 10, pp. 26-31, 2008.
- [7] WHEALS, J. C.; DEANE, M.; DURRY, S.; GRIFFITH, G.; HARMAN, P.; PARKINSON, P.; SHEPHERD, S.; TURNER A.: *Design and Simulation of a Torque Vectoring Rear Axle*, SAE paper # 2006-01-0818, 2006.
- [8] USORO, P.: *Magnetizable Fluid Proves a Plus in a Clutch Situation - New Radiator Fan Drive Boasts the Latest in Cool*, GM Research & Development Note, www.gm.com/company/careers
- [9] ...: *Lord Corporation Magnetorheological (MR) Fluid for Automotive Damping System*, IIR Suspension and Damping Conference, www.lordcorp.com
- [10] CARLSON, J. D.; CATANZARITE, D. M.; ST. CLAIR, K. A.: *Commercial Magneto-Rheological Fluid Devices*, Proc. of the 5th International Conference on ER Fluids, Magneto-Rheological Suspensions and Associated Technology, Sheffield, pp. 20-28, 1995.
- [11] LAMPE, D.: *Untersuchungen zum Einsatz von magnetorheologischen Fluiden in Kupplungen*, Dissertation, TU Dresden, 2000.
- [12] DEUR, J.; LIBL, D.; HEROLD, Z.; HANCOCK, M.; ASSADIAN, F.: *Design and Experimental Characterization of a Magnetorheological Fluid Clutch*, SAE paper No. 2009-01-0142, SAE Congress, Detroit, 2009.
- [13] DEUR, J.; HEROLD, Z.; KOSTELAC, M.: *Modeling of Electromagnetic Circuit of a Magnetorheological Fluid Clutch*, Proc. of IEEE Conference on Control Applications, St. Petersburg, Russia, 2009.
- [14] TAKESUE, N.; FURUSHO, J.; KIYOTA, Y.: *Fast Response MR-Fluid Actuator*, JSME International Journal, Series C, Vol. 47, No. 3, pp. 783-791, 2004.
- [15] PETRIĆ, J.; DEUR, J.; PAVKOVIĆ, D.; MAHALEC, I.; HEROLD, Z.: *Experimental Setup for SI-Engine Modeling and Control Research*, Strojarstvo, Vol. 46, No. 1-3, pp. 39-50, 2004.
- [16] ...: *Magnetic Circuit Desig*, Lord Corporation, www.lordcorp.com
- [17] ...: *MRF-132DG Magneto-Rheological Fluid*, Lord Corporation, www.lordcorp.com
- [18] LEONHARD, W.: *Control of Electrical Drives*, Springer Verlag (3rd edition), 2001.
- [19] ARMSTRONG-HÉLOUVRY, B.; DUPONT, P.; CANUDAS DE WIT, C.: *A Survey of Models, Analysis Tools and Compensation Methods for the Control of Machines With Friction*, Automatica, Vol. 30, pp. 1083-1138, 1994.